Mercury's three-dimensional asymmetric magnetopause

J. Zhong[1], W. X. Wan[1], J. A. Slavin[2], Y. Wei[1], R. L. Lin[3], L. H. Chai[1], J. M. Raines[2], Z. J. Rong[1], X. H. Han[1]

[1]Key Laboratory of Earth and Planetary Physics, Institute of Geology and Geophysics, Chinese Academy of Sciences, Beijing, China.

[2]Department of Atmospheric, Oceanic and Space Sciences, University of Michigan, Ann Arbor, Michigan, USA.

[3]Center for Space Science and Applied Research, Chinese Academy of Sciences, Beijing, China.

Correspondence to: Zhong Jun (j.zhong@mail.iggcas.ac.cn).

This is the author manuscript accepted for publication and has undergone full peer review but has not been through the copyediting, typesetting, pagination and proofreading process, which may lead to differences between this version and the Version of Record. Please cite this article as doi: 10.1002/2015JA021425

Abstract

Mercury's magnetopause is unique in the solar system due to its relatively small size and its close proximity to the Sun. Based on 3 years of MESSENGER orbital Magnetometer and the Fast Imaging Plasma Spectrometer data, the mean magnetopause location was determined for a total of 5694 passes. We fit these magnetopause locations to a three-dimensional non-axially symmetric magnetopause which includes an indentation for the cusp region that has been successfully applied to the Earth. Our model predicts that Mercury's magnetopause is highly indented surrounding the cusp with central depth ~0.64 R_M and large dayside extension. The dayside polar magnetopause dimension is, thus, smaller than the equatorial magnetopause dimension. Cross sections of the dayside magnetopause in planes perpendicular to the Mercury-Sun line are prolate and elongated along the dawn-dusk direction. In contrast, the magnetopause downstream of the terminator plane is larger in the north-south than the east-west directions by a ratio of 2.6 R_M to 2.2 R_M at a distance of 1.5 R_M downstream of Mercury. Due to the northward offset of the internal dipole, the model predicts that solar wind has direct access to the surface of Mercury at middle magnetic latitudes in the southern hemisphere. During extremely high solar wind pressure conditions, the northern hemisphere middle magnetic latitudes may also be subject to direct solar wind impact.

1. Introduction

The planetary magnetopause is a magnetic field and plasma boundary formed by the interaction between solar wind and planetary magnetosphere. Its size and shape provide key clues about the magnetospheric internal structure. Compared to the other planets with an intrinsic magnetosphere in solar system, Mercury is closest to the Sun and is the smallest magnetosphere in size. This makes the Mercury's magnetopause unique in the context of comparative magnetosphere-solar wind interaction study.

Mercury's magnetopause and internal dipole field structure were first detected in 1974-1975 by two Mariner 10 flybys [*Ness et al.*, 1974; *Ness et al.*, 1975]. Recent extensive observations by MErcury Surface, Space ENvironment, GEochemistry, and Ranging (MESSENGER) indicated that Mercury has a dipole field similar to Earth, but its dipole moment is much smaller, 195 nT R_M^3 (where R_M is Mercury' mean radius, 2440 km) with an offset ~0.2 R_M northward from the planetary center [*Alexeev et al.*, 2010; *Anderson et al.*, 2011; *Anderson et al.*, 2012; *Johnson et al.*, 2012]. Such a weak dipole field, combined with the most extreme solar wind driving forces in the solar system, creates a planetary magnetosphere with a size that is about 5% that of the Earth's magnetosphere [*Winslow et al.*, 2013]. MESSENGER observations indicate that Mercury's tiny magnetopause is highly variable and dynamic [e.g., *Slavin et al.*, 2009a; *DiBraccio et al.*, 2013]. Based on the assumption of a rotationally symmetric magnetopause shape, *Winslow et al.* [2013] statistically analyzed the

Mercury's magnetopause responses to solar wind dynamic pressure. They concluded that the magnetopause moves closer to the planet under higher solar wind dynamic pressure but that its shape remains unchanged.

In contrast to the Earth and the outer planets, the weakness of Mercury magnetic field begs the question of whether or not solar wind ram pressure is sufficient to compress the magnetopause to the surface, or to a distance within an ion gyroradius from the surface, leading to direct impact of solar wind on the surface which would cause the sputtering of neutrals and ions [*Killen et al.*, 2001] and space weathering of the regolith [*Domingue et al.*, 2014]. Using pressure balance, *Siscoe and Christopher* [1975] argued that the solar wind pressure is insufficient to depress the subsolar magnetopause to the surface for almost all solar wind pressure conditions. However, it has been argued by *Slavin and Holzer* [1979] that the magnetic reconnection would be more efficient closer to the Sun where the solar wind Alfvén speed is enhanced. On this basis they estimated that the reconnection-driven transfer of magnetic flux from the dayside magnetosphere to the magnetotail, termed "erosion", might expose the surface to direct solar wind impact for a significant portion of the time. On the other hand, *Hood and Schubert* [1979] examined the impact of induction currents driven in Mercury's interior when the solar wind compresses the dayside magnetosphere, but without consideration of reconnection, and concluded that solar wind pressure alone was not likely to drive the magnetopause to the surface. Recently, MESSENGER

observations of the dayside magnetosphere of Mercury during coronal mass ejections and high-speed streams indicate that both effects, erosion and induction, are important, and suggest that at least portions of the surface are exposed, especially in the southern hemisphere where the planetary magnetic field is weakest due to the offset of Mercury's dipole [*Slavin et al.*, 2014].

Previous predictions on the Mercury's magnetopause location [e.g., *Slavin et al.*, 2009b; *Slavin et al.*, 2010; *Johnson et al.*, 2012; *Winslow et al.*, 2013; *Slavin et al.*, 2014] all assumed that the magnetopause shape is axisymmetric about the Sun-dipole center line, i.e., the cross section of the magnetopause is circular. At Earth, the magnetic cusps make the greatest contribution to the three-dimensional shape of the dayside magnetopause. The polar cusps represent indentations upon the magnetopause at the high latitude [e.g., *Dunlop et al.*, 2000; *Zhang et al.*, 2007]. As a consequence, the equatorial dimensions of the dayside magnetopause should exceed the polar dimensions [*Sibeck et al.*, 1991; *Boardsen et al.*, 2000]. Based on the large database of terrestrial magnetopause crossings, the fitted global models [*Lin et al.*, 2010; *Wang et al.*, 2013] clearly show outer cusp indentations with complex dependence on various control parameters.

Apart from the near-cusp indentations, there is also direct observational evidence for the asymmetry of the Earth's magnetopause tail shape, especially during periods of low solar wind Alfvénic Mach numbers [*Lavraud et al.*, 2013] and geomagnetic

storms [*Nakamura et al.*, 1997]. The square of the Alfvénic Mach number is equivalent to the ratio of the dynamic pressure of the solar plasma to the magnetic pressure. During low Alfvénic Mach number, the anisotropic magnetic pressure and its "tension" in the magnetic field draped around the magnetosphere can significantly cause "flattening" of the magnetotail and other departures from axial symmetry [e.g., *Sibeck et al.*, 1985; *Sibeck et al.*, 1986; *Sibeck and Lin*, 2014].

The previous analysis at Earth indicates that a more accurate model of Mercury's magnetopause may result if the assumption of axial symmetry is relaxed. Knowledge of the three-dimensional shape of Mercury's magnetopause and its average size is crucial to extending the understanding of the interaction between the solar wind and the planetary magnetosphere, as well as of changes to Mercury's space environment from solar wind-surface interaction. With 3 years of MESSENGER orbital data from the Magnetometer (MAG) [*Anderson et al.*, 2007] and Fast Imaging Plasma Spectrometer (FIPS) [*Andrews et al.*, 2007] instruments, we identified the mean magnetopause location for a total of 5696 passes. Our statistical analyses indicate that there were strong azimuthal asymmetries and near-cusp indentations at Mercury's magnetopause. A three-dimensional asymmetric model of Mercury's average magnetopause was developed. The model predicts that the average magnetopause would contact the planetary surface at middle magnetic latitudes in the southern hemisphere due to the magnetopause indentation.

2. MESSENGER Magnetopause Observations

The MESSENGER spacecraft was inserted into a highly inclined, eccentric orbit about Mercury in March 2011 [*Solomon et al.*, 2007]. The initial orbit had a 200-km periapsis altitude over 60°N latitude, 15,300 km apoapsis altitude and an 80° inclination to Mercury's equator. The MESSENGER's orbit around the Mercury was approximately fixed in inertial space so that the orbit completes a local-time rotation once every Mercury year (88 Earth days) (see details in [*McAdams et al.*, 2007; *Bedini et al.*, 2012]). The periherm altitude and latitude of the orbit also drifted during every Mercury year. During one Mercury year the MESSENGER orbit varied between two extremes, the dawn-dusk terminator and noon-midnight orbits. When the orbit transitioned to a noon-midnight configuration with periapsis on the dayside (Figure 1 g-h), which are termed "hot" season orbits, MESSENGER passed the dayside magnetopause at low latitude, through the northern cusp, and crossed the nightside high latitude magnetopause. When the orbital periapsis was on the nightside (Figure 2 g-h), which are termed "warm" season orbits, MESSENGER crossed the higher latitude dayside magnetopause. These higher latitude passes often sampled the dayside closed magnetic field regions of the magnetosphere near the cusp region. When the spacecraft orbit transitioned to a dawn-dusk configuration (Figure 3 g-h),

MESSENGER passed the magnetopause flank region close to the day-night terminator.

The change in the orbit's Sun orientation provides excellent spatial coverage of the interaction at the Mercury magnetopause. Figure 1-4 show examples of the magnetopause crossings at dayside low latitude and high latitude, flank region and nightside high latitude, respectively. The magnetic field and spacecraft position data are analyzed in Solar-wind-aberrated Mercury solar magnetospheric (MSM) coordinates. In MSM coordinate system, the X_{MSM} axis is directed from Mercury's offset magnetic dipole center toward the Sun, the Z_{MSM} axis is normal to Mercury's orbital plane and points northward, and the Y_{MSM} axis completes the right-handed system. The MSM coordinates have been rotated for solar wind aberration, then the aberrated positive X_{MSM} is opposite to the solar wind flow in Mercury's frame. An aberration angle was calculated for each MESSENGER orbit using Mercury's instantaneous orbital speed and an average radial solar wind speed of 400 km/s. Due to Mercury's large variation in orbital speed, the aberration angle varied from 5.5°at aphelion to 8.4° at perihelion.

The magnetopause crossings were identified using the magnetic field data or the proton flux data, or both. The principal criterion for magnetopause identification is that the magnetic field undergoes an abrupt transition from a more steady planetary-like field to a more highly fluctuating sheath-like field, and vice versa. The

transition is usually marked by an abrupt change in magnetic field strength and/or direction as the spacecraft crosses the current layer. As examples in Figure 2-4 show, these magnetopauses can be easily identified by clear changes in the magnetic field direction between the magnetosheath and the magnetosphere.

Magnetic field data alone are not always sufficient for identifying magnetopause crossings. For example, strong plasma depletion layers often form just exterior to the subsolar magnetopause due to the low Alfvénic Mach number in solar wind at Mercury [*Gershman et al.*, 2013]. The presence of a plasma depletion layer makes magnetopause identification difficult when there is little change in the magnetic field magnitude and small shear angles between the planetary magnetic field and the draped magnetosheath field. In these cases, the proton flux data from FIPS were used to assist in identifying the crossings. The magnetopause crossings can be identified by a sharp increase in heated ion flux from planetary magnetosphere to the solar wind, and vice versa. An example of such magnetopause identification is shown in Figure 1.

Due to inward-outward magnetopause motions, multiple magnetopause crossings are typically observed (e.g., Figure 2, 4). On each pass, the innermost and outermost crossings are averaged to represent the mean magnetopause location, so that there is only one "point" per pass through the magnetopause inbound or outbound on each orbit. We searched 3 years of MESSENGER orbital data starting on 24 March 2011 and extending through 17 March 2014. This time interval contains one year where the

orbital period is 12 h, and two years where it is 8 h. The difference between these two orbits is that in the 12-h orbit the spacecraft crossed the dayside magnetopause at lower latitudes and the nightside magnetopause farther down the tail than in the 8-h orbit. A total of 5696 magnetopause passes were identified by visual inspection.

At Mercury, the solar wind dynamic pressure strongly controls the magnetopause location [*Winslow et al.*, 2013]. During extremely high solar wind pressure events, the magnetopause crossings were displaced substantially inward from the average boundary and lay very close to Mercury's surface [*Slavin et al.*, 2014]. For the first order of approximation, the upstream solar wind total pressure is balanced by the magnetic pressure of the planetary magnetosphere. Thus the magnetic field intensity just inside the dayside magnetopause is a good indicator of these extreme solar wind pressure events. Using the same criterion as *Slavin et al.* [2014], i.e., the threshold of the magnetic field just inside the magnetopause exceeded 300 nT, we have identified 8 dayside magnetopause passes during extremely high solar wind pressure conditions among 3-year MESSENGER orbital data.

Figure 5a shows the statistical distribution of all average crossings in the terminator solar-wind-aberrated MSM plane. Considering Mercury's highly axially aligned dipolar magnetic field (dipole tilt less than 0.8^{o}) [*Anderson et al.*, 2012], it is expected that the magnetopause possesses considerable north-south symmetry. The three-dimensional scatter plot of these average crossings in the near-Mercury space is

shown in Figure 5b. Note that the magnetopause locations in the southern hemisphere were mirrored to the northern hemisphere. In this manner, the data set provides comprehensive coverage of Mercury's dayside magnetopause boundary surface.

3. Three-dimensional Mercury's magnetopause modeling

We used the following three-dimensional surface function to construct the Mercury magnetopause, including azimuthal asymmetry and near-cusp indentations:

$$r(\theta,\varphi) = r_0\left(\frac{2}{1+\cos\theta}\right)^{\alpha+\beta\cdot\cos^2\varphi} - r_{ind}(\theta,\varphi).$$

The model is described in a spherical coordinate system which has its pole aligned with the X_{MSM} direction, where r is the radial distance from the dipole center, θ is the polar angle (or zenith angle), and φ is the azimuth angle between the projection of r in the Y-Z plane and the direction of the positive Y_{MSM} axis from $-\pi$ and π in clockwise looking from the Mercury to the Sun.

The first term on the right-hand of function describes the azimuthal asymmetry of the magnetopause. This term is expanded from the *Shue et al.* [1997] functional form, in which r_0 is the subsolar magnetopause distance and $\alpha+\beta\cdot\cos^2\varphi$ is the level of tail flaring with respect to the azimuth angle. The parameters α and β govern the level of tail flaring together. $\beta\cdot\cos^2\varphi$ describes the change in tail flaring with respect to the azimuth angle. Note that the cosine- or sine-squared form can well describe the terrestrial magnetopause azimuthal asymmetry [*Lin et al.*, 2010; *Lu et al.*, 2011]. The

level of tail flaring thus in the noon-midnight meridional plane is α and in the equatorial plane is $\alpha+\beta$. Its value reflects the magnetopause shape, determining whether the tail is closed (< 0.5), asymptotes to a finite tail radius (= 0.5), or expands with increasing distance from the Mercury (> 0.5).

$r_{ind}(\theta, \varphi)$ describes the magnetopause near-cusp indentations and is expressed by the form of a two-dimensional Gaussian function:

$$r_{ind}(\theta,\varphi) = \sum_{i=n,s} d_i \cdot exp\left[-\frac{1}{2}\left(\frac{\theta-\theta_i}{\Delta_{\theta_i}}\right)^2 - \frac{1}{2}\left(\frac{\varphi-\varphi_i}{\Delta_{\varphi_i}}\right)^2\right].$$

In this Gaussian function, the parameters directly represent the location and the shape of the indentations. The parameters d_i, θ_i, and φ_i represent the central depth, the polar and azimuthal locations of the indentation, respectively, while Δ_{θ_i} and Δ_{φ_i} represent the polar and azimuthal extensions, respectively. All angles are in radians. The subscript *i* equaling *n* (*s*) represents the north (south) near-cusp indentation. Considering the Mercury's axially aligned dipolar magnetic field [*Anderson et al.*, 2012], the north and south magnetopause indentations are expected to be located at azimuth angle $\varphi_0 = \pm\pi/2$ with a north-south symmetrical shape, i.e., $d_n=d_s=d_0$, $\theta_n=\theta_s=\theta_0$, $\Delta_{\theta_n}=\Delta_{\theta_s}=\Delta_\theta$, $\Delta_{\varphi_n}=\Delta_{\varphi_s}=\Delta_\varphi$. Thus, we define 7 configuration parameters (r_0, α, β, d_0, θ_0, Δ_θ, Δ_φ) to describe the three-dimensional asymmetric Mercury's magnetopause surface. The function can be simplified as:

$$r_{ind}(\theta,\varphi) = d_0 \cdot exp\left[-\frac{1}{2}\left(\frac{\theta-\theta_0}{\Delta_\theta}\right)^2\right] \cdot \sum_{\varphi_0=\pm\pi/2} exp\left[-\frac{1}{2}\left(\frac{\varphi-\varphi_0}{\Delta_\varphi}\right)^2\right].$$

The three-dimensional Mercury's magnetopause model was developed by fitting to MESSENGER magnetopause crossings. Here the magnetopause crossings sunward of $X_{MSM} \sim -2\ R_M$ were used to construct the average magnetopause surface. This is because MESSENGER's orbit did not take it sufficiently far exterior to the nominal magnetopause beyond $X_{MSM} \sim -2\ R_M$, which would lead to an orbital bias in determination of average magnetopause size and shape. In addition, to get the average magnetopause shape, 8 dayside magnetopause crossings during extremely high solar wind pressure conditions were also excluded. During these extreme events, the northern cusp becomes unusually broad and deep [*Slavin et al.*, 2014], which would lead the average depth of the near-cusp indentation that can not be accurately modeled.

By the nonlinear least-squares method with trust-region fitting algorithm [*Coleman and Li*, 1996], the best fit configuration parameters to the MESSENGER magnetopause crossings are presented in Figure 5 caption. The least squares solution used minimizes the root mean square (RMS) residual of the perpendicular distance from the magnetopause observation to the fitted surface. From the fitted model, the cross sections of magnetopause at different polar and azimuthal angles with the same interval are shown in Figure 5b and projected in Figure 5a in Y-Z plane. Mercury's magnetopause near-cusp geometry and the azimuthal asymmetry are well described by this model. The best-fit RMS error of perpendicular displacement obtained here is

0.20 R_M. Note that we also tested the previous axially symmetric magnetopause model, established by *Winslow et al*. [2013], by fitting, and found a RMS error of perpendicular displacement 0.27 R_M. The reduced RMS error in our model indicates that the three-dimensional magnetopause model, including azimuthal asymmetry and near-cusp indentations, is more accurate for representing the Mercury's magnetopause.

4. Near-cusp indentation

Previous MESSENGER low altitude observations show that the Mercury northern cusp is highly variable region [*Winslow et al.*, 2012; *Raines et al.*, 2014]. Especially, during extreme solar wind dynamic pressure events, the cusp becomes unusually broad and deep [*Slavin et al.*, 2014]. Within and adjacent to the cusp, it appears largely made up of brief (~1-2 seconds) diamagnetic decreases which are termed cusp plasma filaments [*Slavin et al.*, 2014]. The presence of these isolated cusp filaments is also seen in an example of dayside, high latitude magnetopause crossings shown in Figure 2. These cusp properties are characterized by diamagnetic depressions in the magnetic field intensity and/or the enhanced flux of solar wind protons [*Zurbuchen et al.*, 2011; *Winslow et al.*, 2012; *Raines et al.*, 2014; *Slavin et al.*, 2014]. The magnetopause indentation is formed by magnetosheath-cusp interaction and extends to high-latitude regions. The interface between the cusp and

the magnetosheath is sometimes called the turbulence boundary layer [*Savin et al.*, 2005]. Due to orbit inclination, MESSENGER seldom passed through this interface above the cusp center. But during "warm" season orbits, MESSENGER typically passed through the high-latitude magnetopause between magnetosheath and dayside magnetospheric closed field line region which is termed "high-latitude trapping region" (see Figure 1 in [*Zhang et al.*, 2007]). An example of such near-cusp magnetopause passes is shown in Figure 2. This boundary can be easily identified because the ion flux in the high-latitude trapping region is much lower than that in the magnetosheath and there is a sharp transition in the magnetic field.

To better understand the three-dimensional magnetopause geometry near the cusp, we have statistically investigated the spatial variation of the near-cusp indentation in both the polar direction and the azimuthal direction. The indentation depths are defined as the differences between the average azimuthal asymmetric magnetopause model, $r_0 \left(\frac{2}{1+\cos\theta}\right)^{\alpha+\beta\cdot\cos^2\varphi}$, and the radial distance of observed crossings, $r_{obs}(\theta, \varphi)$. The magnetopause near-cusp indentation can be analyzed using Figure 6. Figure 6a and 6b show the indentation depths in the conic plane near the $\theta = \theta_0$ and in the azimuthal plane near $\varphi = \pi/2$, respectively. The θ_0 is the polar location of the indentation center, and its value is 1.00 (57.3°) from the fitted model. The indentation depths are scatter plotted as a function of the angular distance from the indentation center, the angle between the radial direction $r_{obs}(\theta, \varphi)$ and the direction of the

indentation center $r(\theta_0, \varphi_0)$. From Figure 6, the indentations in Mercury's magnetopause surrounding the cusp are evident in both polar and azimuthal extensions. The plotted solid red curves in Figure 6 are calculated from the model to emphasize this trend.

The magnetopause indentation spreads over a large area on the dayside. Predicted from the two-dimensional Gaussian model, the full-width of the azimuthal (Figure 6a) and polar (Figure 6b) extensions are $2.355 \cdot \Delta_{\varphi} \approx 1.13$ (65°) and $2.355 \cdot \Delta_{\theta} \approx 0.68$ (39°), respectively. The indentation depth gradually increased to the ~ 0.64 R_M when close to the center of the indentation. Applying linear scaling by factor of ~8 [*Ogilvie et al.*, 1977], the near-cusp indentation obtained here yields a depth corresponding to the terrestrial case of 5.1 R_E. This value is larger than average depth ~ 2.5-3 R_E at the Earth [e.g., *Šafránková et al.*, 2005; *Lin et al.*, 2010]. Note that MESSENGER crossed the indentation center near its orbital perigee, and that may introduce orbital bias in the determination of its indentation depth. The depth of the indentation from the model may be biased slightly toward lower altitudes. The reader is referred to *Lin et al.* [2010] for additional discussion concerning magnetopause indentations.

The variability in the near-cusp magnetopause is expected to arise from constantly changing solar wind conditions and magnetospheric dynamics. The dayside magnetopause crossings during extremely high solar wind pressure conditions are green colored in Figure 6b. It can be seen that these near-cusp magnetopause

crossings were unusually deep with respect to the average model.

5. Magnetopause azimuthal asymmetry

Both dayside and nightside magnetopause show strong azimuthal asymmetries. The locations of MESSENGER magnetopause crossings in the Y-Z plane at X_{MSM}=1 R_M, 0 and −1.5 R_M are shown in Figure 7. To emphasize the cross-sectional shape, the two-dimensional cut from the model was also plotted (red curve). Due to the near-cusp indentation, the dayside magnetopause cross section is elongated along the dawn-dusk direction (Figure 7a). On average, the dayside magnetopause equatorial dimension exceeds the polar dimension by 60% at X_{MSM}= 1 R_M.

At the terminator plane, the magnetopause crossings are only sampled in the flank region (Figure 7b). This is due to MESSENGER's highly inclined, eccentric orbit. These flank region crossings are sampled in a distance range of ~ 1.5 to 2.5 R_M. From the model, the magnetopause are nearly circular at the terminator. The average radius is about 2 R_M.

In contrast, the magnetopause downstream of the terminator plane is larger in the north-south than the east-west directions. From the model, the magnetopause tail flaring changes with respect to the azimuth angle. The level of tail flaring in the noon-midnight meridional plane is 0.49, which very close to the previous rotationally symmetric magnetopause model [*Winslow et al.*, 2013]. The value close to 0.5

suggests a transition from an open to a closed magetospheric cavity on the nightside. But in the equatorial plane, the level of tail flaring is much less (0.39), which indicates the magnetopause in this plane would be closed in the tail. As shown in Figure 7c, at X_{MSM}= −1.5 R_M, the magnetotail radii are on average about 2.6 R_M in the noon-midnight meridional plane but 2.2 R_M in the equatorial plane. Applying the linear scaling law [*Ogilvie et al.*, 1977], the result from here yields asymmetry corresponding to the terrestrial case of 3.2 R_E at near-Earth tail X ~ −12 R_E. This differs from the near-Earth tail magnetopause where the cross-section shape is generally near circular due to high solar wind Alfvénic Mach number [*Lavraud et al.*, 2013].

We point out that although we performed fitted data selection to avoid the orbital bias effects, there still exists some orbital biases at nightside magnetopause. These can be found in the low-latitude and high-latitude magnetopause observations which were less frequently encountered than the mid-latitude magnetopause. However, the model well fits the mid-latitude magnetopause. The asymmetry between the polar and the equatorial tail magnetopause (0.4 R_M) is much larger than the standard deviation (0.2 R_M). To confirm the reliability of the surface model, we used ellipse to fit the mid-latitude of magnetopause crossings at X_{MSM}= −1.5 R_M (Figure 7c). The semi-major axis of fitted ellipse is located in north-south direction. The result of ellipse fitting confirmed that the tail azimuthal asymmetry is indeed existed.

6. When and where does the solar wind impact the planet?

As described in the introduction, the possibility that the solar wind directly strikes the planetary dayside surface remains a topic of considerable interest and controversy [*Domingue et al.*, 2014]. The problem is that the MESSENGER orbital observations can not provide direct observations of the magnetopause intersecting the planetary surface. Based on the assumption of rotationally symmetric magnetopause shape, *Winslow et al.* [2013] concluded that the magnetopause moves closer to the planet under higher solar wind dynamic pressure, but its shape remains unchanged. Using Winslow et al.'s rotationally symmetric magnetopause model, *Slavin et al.* [2014] predicted that during coronal mass ejections and high-speed streams the magnetopause may have intersected the planetary surface in the southern hemisphere, where the planetary magnetic field is weakest due to the offset of Mercury's dipole. Here we further take into consideration the three-dimensional asymmetries of the Mercury's magnetopause. Surrounding the polar cusps, the magnetopause is highly indented. Our results suggest that the magnetopause surface geometry near the cusp is so important that it is required for accurate predictions of direct solar wind impact.

The magnetopause locations in the equatorial and polar planes relative to Mercury's surface are shown in Figure 8. The dayside polar magnetopause dimensions are smaller than the equatorial magnetopause dimensions. The magnetopause

crossings close to cusp regions (red crosses) are observed at distances closer to the Mercury surface than those in the equatorial plane (blue crosses). The average location of the polar magnetopause from the model is plotted in the Figure 8 (thick red line). Mercury's surface north of the magnetic equator is shown separately from the surface south of the magnetic equator. This is due to the strong effect of the northward dipole offset (~ 0.2 R_M) on the magnetopause altitude. With assumption of north-south symmetry of the magnetopause shape, the model predicts that the average magnetopause intersected the planetary surface in the southern hemisphere. Those magnetopause crossings observed near the north cusp region are expected to make contact with the surface of Mercury in the southern hemisphere, at middle magnetic latitudes. Considering a large extent of the indentation, large areas in this region could be directly exposed to the shocked solar wind.

During extreme solar wind conditions, the locations of the magnetopause were in close proximity to the high latitudes of the northern planetary surface (green crosses in Figure 8). In some cases, the dayside magnetosphere is highly compressed and MESSENGER misses the dayside magnetosphere and passes directly from the dayside magnetosheath through the post-cusp region into the nightside high latitude magnetosphere. An example of such a magnetopause crossing is shown in Figure 9. On 1 December 2013, the MESSENGER orbit is lying close to the noon-midnight plane (Figure 9g-9h). MESSENGER crossed the bow shock from the solar wind into

the magnetosheath at 01:20:20UT. The bow shock location is displaced to an unusually low altitude from the average position [*Winslow et al.*, 2013]. The highly fluctuating magnetic field (Figure 9a-9e) and heated ion flux (Figure 9f) indicate the spacecraft was situated in the magnetosheath until it crossed the magnetopause at 01:35:40UT. Adjacent to the magnetosphere, MESSENGER measured the planetary field in excess of 400 nT. It was oriented largely in the $+B_X$ and $-B_Z$ direction. The vector plots of the magnetic field (Figure 9f-9g) clearly show these field lines steadily point southward and dipole-center-ward in the noon-midnight plane. The geometry of the field along the orbit suggests that the spacecraft passed directly from the dayside magnetosheath to the magnetopause in the northern tail lobe. In this case, the observed local magnetopause was located 0.14 R_M above the Mercury's northern surface at middle latitudes, i.e., 0.94 R_M distance from the planetary magnetic dipole. It is most likely that the magnetopause would contact with the surface of Mercury at lower magnetic latitudes in the northern hemisphere, or at least be located at a distance lower than 0.14 R_M.

These magnetopause crossings imply that the middle latitudes of Mercury's surface in the northern hemisphere may be another region where the solar wind directly impacts the planet during the extreme solar wind events. When the magnetopause approaches close to the surface of Mercury, the solar wind impact will lead to planetary ion sputtering that rapidly changes in Mercury's exosphere [*Killen et*

al., 2001]. To confirm our prediction, further analysis of the planetary ions spatial distribution response to these extreme solar wind events is required.

7. Discussion

Applying the linear scaling law [*Ogilvie et al.*, 1977], the average asymmetries of the Mercury's magnetopause are more significant than Earth. The spread in the magnetopause locations, especially during the extremely high solar wind pressure conditions, represent large variations in Mercury's three-dimensional magnetosphere. *Slavin et al*. [2014] investigated three extreme solar wind dynamic pressure events accompanied by strong magnetopause reconnection and found that the low-altitude cusp region becomes unusually broad and deep. Here we found the typical high-latitude near-cusp magnetopause boundary locations are also much deeper than the average magnetopause location during similar extreme events. The solar wind dynamic pressure exerts a primary control on magnetopause location [*Winslow et al.*, 2013]. At Mercury, the IMF conditions are also expected to play a major role in the three-dimensional magnetopause shape due to the high reconnection rate at Mercury's magnetopause [*Slavin et al.*, 2009a; *DiBraccio et al.*, 2013; *Slavin et al.*, 2014].

The magnetopause near-cusp indentation should have complex dependence on the IMF conditions. At Earth, the IMF B_Z and/or B_Y component primarily control the location and extent of the indentation [e.g., *Boardsen et al.*, 2000; *Šafránková et al.*,

2005; *Zhang et al.*, 2007; *Lu et al.*, 2013]. Recent global models [*Lin et al.*, 2010; *Liu et al.*, 2012] predicted that the Earth's dipole tilt angle also significantly affects the cusp locations and the degree of asymmetry between the Northern and Southern hemispheres. At Mercury the effect of dipole tilt can be neglected due to its axially aligned dipolar magnetic field [*Anderson et al.*, 2012]. Unlike Earth, The strong radial IMF commonly occurs at Mercury [*Korth et al.*, 2011]. The increasing fraction of IMF B_X is therefore expected to significantly control the reconnection topology on the Mercury's magnetosphere [*Kabin et al.*, 2000; *Belenkaya et al.*, 2013] and thus influence the near-cusp magnetopause North-South asymmetry. The effect of the more radial IMF on reconnection is seen in the strong control of IMF B_X on reconnection just tail ward of the two cusps [*Slavin et al.*, 2012]. The magnetosheath plasma being injected into the cusp and carried into the plasma mantle by this "lobe reconnection" caused by strong B_X is probably an important factor in the depth of the cusp signatures.

As mentioned in the introduction, the draping of the magnetosheath magnetic field lines may exert an anisotropic pressure on the tail magnetopause that deforms its shape. Recent global MHD simulations predicted that the cross-sectional shape in the Earth's magnetotail is controlled by the IMF clock angle, i.e., the cross sections elongated in the direction parallel to the component of the IMF in the plane perpendicular to the Sun-Earth line [*Lu et al.*, 2013; *Sibeck and Lin*, 2014; *Wang et al.*,

2014]. This effect is particularly noticeable at near-Earth tail during intervals of low solar wind Alfvénic Mach number [*Lavraud and Borovsky*, 2008; *Lavraud et al.*, 2013]. At Mercury's orbit, the mean IMF intensity is 3-6 times more intense [*Burlaga*, 2001] and Alfvénic Mach number is about half of that experienced at the Earth [*Slavin and Holzer*, 1981]. Indeed, *Ridley et al.* [2007] and *Sarantos and Slavin* [2009] predict that Alfvén wings may sometimes form at Earth and Mercury, respectively, during the most extreme low Alfvénic Mach number conditions. Although Alfvén wings have not yet been found at Mercury, the global simulations by *Ridley* [2007] show that north-south dimensions of magnetotails during southward or northward IMF are predicted to grow as Alfvénic Mach number decreases to the values found along the Mercury orbit. Nevertheless, the clock angle of IMF at Mercury's orbit was more in the dawn-dusk direction than in the north-south direction [*Korth et al.*, 2011]. Considering these solar wind and IMF conditions, one may expect that the Mercury's magnetotail radius in the dawn-dusk would be larger than that in the north-south. However, our three-dimensional magnetopause model suggests that Mercury's magnetotail radius is larger in the north-south direction than the dawn-dusk direction, though there exists potential orbital bias effects. The statistical analyses of Mercury's magnetopause at $X_{MSM}= -1.5\ R_M$ further confirmed that the cross-section shape is elongated in the north-south direction (Figure 7c). The average azimuthal asymmetry of the Mercury's tail magnetopause shown here can not be interpreted by the tail

"flattening" due to IMF draping or Alfvén wings. One of potential explanations is that the dipole field is more intense at higher latitudes, so that the magnetosphere is inflated in the north-south than in the dawn-dusk region. This elongation in the north-south direction is presented in a global MHD simulation of Earth's magnetosphere under zero IMF [*Sonnerup et al.*, 2001]. Other effects which may lead to this deformation of Mercury's magnetopause should be investigated.

7. Summary

We statistically studied the MESSENGER magnetopause mean crossings for 5696 inbound/outbound passes from March 2011 through March 2014. A three-dimensional asymmetric model of Mercury's average magnetopause was developed. We found that both the near-cusp indentation and azimuthal asymmetry at downstream of the terminator plane contribute to the three-dimensional shape of magnetopause. These asymmetries are more significant than at Earth. The results suggest that the near-cusp magnetopause geometry should be taken into account for understanding the response of Mercury's space environment to direct solar wind-planet interaction. During extremely high solar wind pressure conditions, not only the southern hemisphere but also the northern hemisphere mid-latitude surface may be subject to direct solar wind impact. Deeper understanding of Mercury's highly dynamic magnetopause, including its asymmetries, is likely to come from additional

comparative studies with Earth.

Acknowledgement.

This work is supported by the National Natural Science Foundation of China (41404137, 41321003, 41131066, 41474155) and the National Important Basic Research Project (2011CB811405). One of the authors (JAS) is supported by the NASA Solar System Workings program through grant NNX15AH28G and the Heliophysics Supporting Research program through grant NNX15AJ68G.

MESSENGER MAG and FIPS data used in this study are available from the Planetary Data System (http://ppi.pds.nasa.gov/).

References

Alexeev, I. I., et al. (2010), Mercury's magnetospheric magnetic field after the first two MESSENGER flybys, *Icarus*, *209*(1), 23-39, doi:10.1016/j.icarus.2010.01.024.

Anderson, B., M. Acuña, D. Lohr, J. Scheifele, A. Raval, H. Korth, and J. Slavin (2007), The Magnetometer instrument on MESSENGER, *Space Sci. Rev.*, *131*(1-4), 417-450, doi:10.1007/s11214-007-9246-7.

Anderson, B. J., C. L. Johnson, H. Korth, M. E. Purucker, R. M. Winslow, J. A. Slavin, S. C. Solomon, R. L. McNutt, J. M. Raines, and T. H. Zurbuchen (2011), The

global magnetic field of Mercury from MESSENGER orbital observations, *Science*, *333*(6051), 1859-1862, doi:10.1126/science.1211001.

Anderson, B. J., C. L. Johnson, H. Korth, R. M. Winslow, J. E. Borovsky, M. E. Purucker, J. A. Slavin, S. C. Solomon, M. T. Zuber, and R. L. McNutt (2012), Low-degree structure in Mercury's planetary magnetic field, *J. Geophys. Res.*, *117*, E00L12, doi:10.1029/2012je004159.

Andrews, G. B., et al. (2007), The Energetic Particle and Plasma Spectrometer instrument on the MESSENGER spacecraft, *Space Sci. Rev.*, *131*(1-4), 523-556, doi:10.1007/s11214-007-9272-5.

Bedini, P. D., S. C. Solomon, E. J. Finnegan, A. B. Calloway, S. L. Ensor, R. L. McNutt, B. J. Anderson, and L. M. Prockter (2012), MESSENGER at Mercury: A mid-term report, *Acta Astronaut*, *81*, 369-379, doi:10.1016/j.actaastro.2012.07.011.

Belenkaya, E. S., I. I. Alexeev, J. A. Slavin, and M. S. Blokhina (2013), Influence of the solar wind magnetic field on the Earth and Mercury magnetospheres in the paraboloidal model, *Plan. Space Sci.*, *75*(0), 46-55, doi:10.1016/j.pss.2012.10.013.

Boardsen, S. A., T. E. Eastman, T. Sotirelis, and J. L. Green (2000), An empirical model of the high-latitude magnetopause, *J. Geophys. Res. Space Physics*, *105*(A10), 23193-23219, doi:10.1029/1998JA000143.

Burlaga, L. F. (2001), Magnetic fields and plasmas in the inner heliosphere: Helios results, *Plan. Space Sci.*, *49*(14-15), 1619-1627,

doi:10.1016/S0032-0633(01)00098-8.

Coleman, T. F., and Y. Li (1996), An Interior Trust Region Approach for Nonlinear Minimization Subject to Bounds, *SIAM Journal on Optimization*, *6*(2), 418-445, doi:doi:10.1137/0806023.

DiBraccio, G. A., J. A. Slavin, S. A. Boardsen, B. J. Anderson, H. Korth, T. H. Zurbuchen, J. M. Raines, D. N. Baker, R. L. McNutt, and S. C. Solomon (2013), MESSENGER observations of magnetopause structure and dynamics at Mercury, *J. Geophys. Res. Space Physics*, *118*(3), 997-1008, doi:10.1002/jgra.50123.

Domingue, D., et al. (2014), Mercury's weather-beaten surface: understanding Mercury in the context of Lunar and asteroidal space weathering studies, *Space Sci. Rev.*, *181*(1-4), 121-214, doi:10.1007/s11214-014-0039-5.

Dunlop, M. W., P. J. Cargill, T. J. Stubbs, and P. Woolliams (2000), The high-altitude cusps: HEOS 2, *J. Geophys. Res. Space Physics*, *105*(A12), 27509-27517, doi:10.1029/2000JA900084.

Gershman, D. J., J. A. Slavin, J. M. Raines, T. H. Zurbuchen, B. J. Anderson, H. Korth, D. N. Baker, and S. C. Solomon (2013), Magnetic flux pileup and plasma depletion in Mercury's subsolar magnetosheath, *J. Geophys. Res. Space Physics*, *118*(11), 2013JA019244, doi:10.1002/2013JA019244.

Hood, L. L., and G. Schubert (1979), Inhibition of solar wind impingement on mercury by planetary induction currents, *J. Geophys. Res. Space Physics*, *84*(A6),

2641-2647, doi:10.1029/JA084iA06p02641.

Johnson, C. L., et al. (2012), MESSENGER observations of Mercury's magnetic field structure, *J. Geophys. Res. Planets*, *117*(E12), E00L14, doi:10.1029/2012je004217.

Kabin, K., T. I. Gombosi, D. L. DeZeeuw, and K. G. Powell (2000), Interaction of Mercury with the solar wind, *Icarus*, *143*(2), 397-406, doi:10.1006/icar.1999.6252.

Killen, R. M., A. E. Potter, P. Reiff, M. Sarantos, B. V. Jackson, P. Hick, and B. Giles (2001), Evidence for space weather at Mercury, *J. Geophys. Res. Planets*, *106*(E9), 20509-20525, doi:10.1029/2000JE001401.

Korth, H., B. J. Anderson, T. H. Zurbuchen, J. A. Slavin, S. Perri, S. A. Boardsen, D. N. Baker, S. C. Solomon, and R. L. McNutt Jr (2011), The interplanetary magnetic field environment at Mercury's orbit, *Plan. Space Sci.*, *59*(15), 2075-2085, doi:10.1016/j.pss.2010.10.014.

Lavraud, B., and J. E. Borovsky (2008), Altered solar wind-magnetosphere interaction at low Mach numbers: Coronal mass ejections, *J. Geophys. Res. Space Physics*, *113*(A9), A00B08, doi:10.1029/2008JA013192.

Lavraud, B., et al. (2013), Asymmetry of magnetosheath flows and magnetopause shape during low Alfvén Mach number solar wind, *J. Geophys. Res. Space Physics*, *118*(3), 1089-1100, doi:10.1002/jgra.50145.

Lin, R. L., X. X. Zhang, S. Q. Liu, Y. L. Wang, and J. C. Gong (2010), A three-dimensional asymmetric magnetopause model, *J. Geophys. Res. Space*

Physics, *115*(A4), A04207, doi:10.1029/2009JA014235.

Liu, Z. Q., J. Y. Lu, K. Kabin, Y. F. Yang, M. X. Zhao, and X. Cao (2012), Dipole tilt control of the magnetopause for southward IMF from global magnetohydrodynamic simulations, *J. Geophys. Res. Space Physics*, *117*(A7), A07207, doi:10.1029/2011JA017441.

Lu, J. Y., Z. Q. Liu, K. Kabin, M. X. Zhao, D. D. Liu, Q. Zhou, and Y. Xiao (2011), Three dimensional shape of the magnetopause: Global MHD results, *J. Geophys. Res. Space Physics*, *116*(A9), A09237, doi:10.1029/2010JA016418.

Lu, J. Y., Z. Q. Liu, K. Kabin, H. Jing, M. X. Zhao, and Y. Wang (2013), The IMF dependence of the magnetopause from global MHD simulations, *J. Geophys. Res. Space Physics*, *118*(6), 3113-3125, doi:10.1002/jgra.50324.

McAdams, J. V., R. W. Farquhar, A. H. Taylor, and B. G. Williams (2007), MESSENGER mission design and navigation, *Space Sci. Rev.*, *131*(1-4), 219-246, doi:10.1007/s11214-007-9162-x.

Nakamura, R., S. Kokubun, T. Mukai, and T. Yamamoto (1997), Changes in the distant tail configuration during geomagnetic storms, *J. Geophys. Res. Space Physics*, *102*(A5), 9587-9601, doi:10.1029/97JA00095.

Ness, N. F., K. W. Behannon, R. P. Lepping, Y. C. Whang, and K. H. Schatten (1974), Magnetic field observations near Mercury: Preliminary results from Mariner 10, *Science*, *185*(4146), 151-160, doi:10.1126/science.185.4146.151.

Ness, N. F., K. W. Behannon, R. P. Lepping, and Y. C. Whang (1975), Magnetic field of Mercury confirmed, *Nature*, *255*(5505), 204-205.

Ogilvie, K. W., J. D. Scudder, V. M. Vasyliunas, R. E. Hartle, and G. L. Siscoe (1977), Observations at planet Mercury by Plasma Electron Experiment - Mariner-10, *J. Geophys. Res.*, *82*(13), 1807-1824, doi:Doi 10.1029/Ja082i013p01807.

Raines, J. M., D. J. Gershman, J. A. Slavin, T. H. Zurbuchen, H. Korth, B. J. Anderson, and S. C. Solomon (2014), Structure and dynamics of Mercury's magnetospheric cusp: MESSENGER measurements of protons and planetary ions, *J. Geophys. Res. Space Physics*, *119*(8), 2014JA020120, doi:10.1002/2014JA020120.

Ridley, A. J. (2007), Alfvén wings at Earth's magnetosphere under strong interplanetary magnetic fields, *Ann. Geophys.*, *25*(2), 533-542, doi:10.5194/angeo-25-533-2007.

Šafránková, J., Š. Dušík, and Z. Němeček (2005), The shape and location of the high-latitude magnetopause, *Adv. Space Res.*, *36*(10), 1934-1939, doi:10.1016/j.asr.2004.05.009.

Sarantos, M., and J. A. Slavin (2009), On the possible formation of Alfvén wings at Mercury during encounters with coronal mass ejections, *Geophys. Res. Lett.*, *36*(4), L04107, doi:10.1029/2008GL036747.

Savin, S., et al. (2005), Magnetosheath interaction with the high latitude magnetopause, in *The magnetospheric cusps: Structure and dynamics*, edited by T.

Fritz and S. Fung, pp. 95-133, Springer Netherlands, doi:10.1007/1-4020-3605-1_5.

Shue, J. H., J. K. Chao, H. C. Fu, C. T. Russell, P. Song, K. K. Khurana, and H. J. Singer (1997), A new functional form to study the solar wind control of the magnetopause size and shape, *J. Geophys. Res. Space Physics*, *102*(A5), 9497-9511, doi:10.1029/97JA00196.

Sibeck, D. G., G. L. Siscoe, J. A. Slavin, E. J. Smith, B. T. Tsurutani, and R. P. Lepping (1985), The distant magnetotail's response to a strong interplanetary magnetic field By: Twisting, flattening, and field line bending, *J. Geophys. Res. Space Physics*, *90*(A5), 4011-4019, doi:10.1029/JA090iA05p04011.

Sibeck, D. G., G. L. Siscoe, J. A. Slavin, and R. P. Lepping (1986), Major flattening of the distant geomagnetic tail, *J. Geophys. Res. Space Physics*, *91*(A4), 4223-4237, doi:10.1029/JA091iA04p04223.

Sibeck, D. G., R. E. Lopez, and E. C. Roelof (1991), Solar wind control of the magnetopause shape, location, and motion, *J. Geophys. Res. Space Physics*, *96*(A4), 5489-5495, doi:10.1029/90JA02464.

Sibeck, D. G., and R. Q. Lin (2014), Size and shape of the distant magnetotail, *J. Geophys. Res. Space Physics*, *119*(2), 2013JA019471, doi:10.1002/2013JA019471.

Siscoe, G., and L. Christopher (1975), Variations in the solar wind stand-off distance at Mercury, *Geophys. Res. Lett.*, *2*(4), 158-160, doi:10.1029/GL002i004p00158.

Slavin, J. A., and R. E. Holzer (1979), The effect of erosion on the solar wind stand-off distance at Mercury, *J. Geophys. Res. Space Physics*, *84*(A5), 2076-2082, doi:10.1029/JA084iA05p02076.

Slavin, J. A., and R. E. Holzer (1981), Solar wind flow about the terrestrial planets 1. Modeling bow shock position and shape, *J. Geophys. Res. Space Physics*, *86*(A13), 11401-11418, doi:10.1029/JA086iA13p11401.

Slavin, J. A., et al. (2009a), MESSENGER observations of magnetic reconnection in Mercury's magnetosphere, *Science*, *324*(5927), 606-610, doi:10.1126/science.1172011.

Slavin, J. A., et al. (2009b), MESSENGER observations of Mercury's magnetosphere during northward IMF, *Geophys. Res. Lett.*, *36*(2), L02101, doi:10.1029/2008GL036158.

Slavin, J. A., et al. (2010), MESSENGER observations of extreme loading and unloading of Mercury's magnetic tail, *Science*, *329*(5992), 665-668, doi:10.1126/science.1188067.

Slavin, J. A., et al. (2012), MESSENGER observations of a flux-transfer-event shower at Mercury, *J. Geophys. Res. Space Physics*, *117*(A12), A00M06, doi:10.1029/2012ja017926.

Slavin, J. A., et al. (2014), MESSENGER observations of Mercury's dayside magnetosphere under extreme solar wind conditions, *J. Geophys. Res. Space*

Physics, 2014JA020319, doi:10.1002/2014JA020319.

Solomon, S., R. McNutt, Jr., R. Gold, and D. Domingue (2007), MESSENGER mission overview, *Space Sci. Rev.*, *131*(1-4), 3-39, doi:10.1007/s11214-007-9247-6.

Sonnerup, B. U. Ö., K. D. Siebert, W. W. White, D. R. Weimer, N. C. Maynard, J. A. Schoendorf, G. R. Wilson, G. L. Siscoe, and G. M. Erickson (2001), Simulations of the magnetosphere for zero interplanetary magnetic field: The ground state, *J. Geophys. Res. Space Physics*, *106*(A12), 29419-29434, doi:10.1029/2001JA000124.

Wang, J. Y., C. Wang, Z. H. Huang, and T. R. Sun (2014), Effects of the interplanetary magnetic field on the twisting of the magnetotail: Global MHD results, *J. Geophys. Res. Space Physics*, *119*(3), 1887-1897, doi:10.1002/2013JA019257.

Wang, Y., D. G. Sibeck, J. Merka, S. A. Boardsen, H. Karimabadi, T. B. Sipes, J. Šafránková, K. Jelínek, and R. Lin (2013), A new three-dimensional magnetopause model with a support vector regression machine and a large database of multiple spacecraft observations, *J. Geophys. Res. Space Physics*, *118*(5), 2173-2184, doi:10.1002/jgra.50226.

Winslow, R. M., C. L. Johnson, B. J. Anderson, H. Korth, J. A. Slavin, M. E. Purucker, and S. C. Solomon (2012), Observations of Mercury's northern cusp region with MESSENGER's Magnetometer, *Geophys. Res. Lett.*, *39*(8), L08112,

doi:10.1029/2012gl051472.

Winslow, R. M., B. J. Anderson, C. L. Johnson, J. A. Slavin, H. Korth, M. E. Purucker, D. N. Baker, and S. C. Solomon (2013), Mercury's magnetopause and bow shock from MESSENGER Magnetometer observations, *J. Geophys. Res. Space Physics*, *118*(5), 2213-2227, doi:10.1002/jgra.50237.

Zhang, H., M. W. Dunlop, Q. G. Zong, T. A. Fritz, A. Balogh, and Y. Wang (2007), Geometry of the high-latitude magnetopause as observed by Cluster, *J. Geophys. Res. Space Physics*, *112*(A2), A02204, doi:10.1029/2006JA011774.

Zurbuchen, T. H., et al. (2011), MESSENGER observations of the spatial distribution of planetary ions near Mercury, *Science*, *333*(6051), 1862-1865, doi:10.1126/science.1211302.

Figure 1.

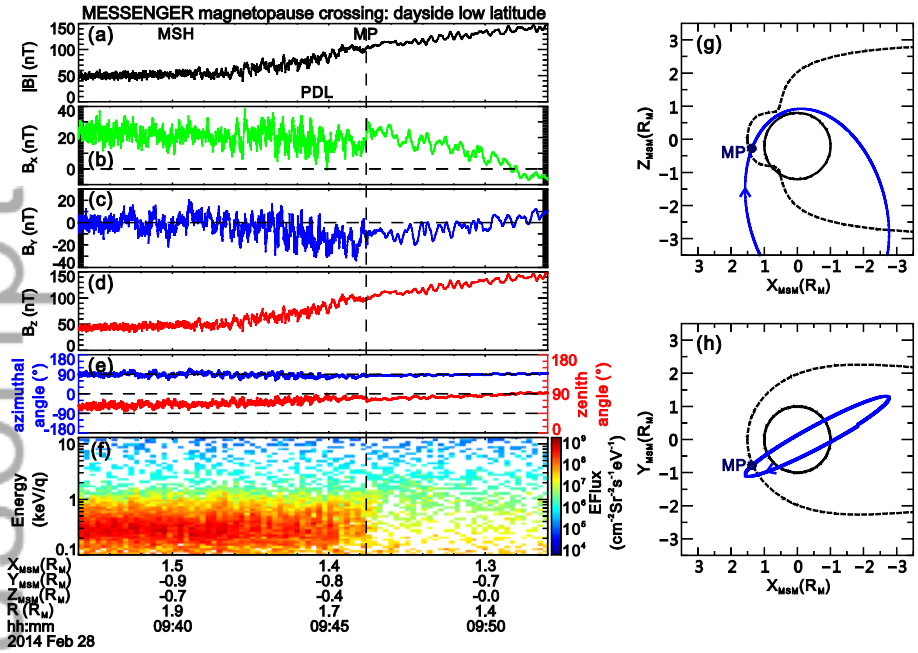

Figure 1. Example of MESSENGER inbound passage from magnetosheath through the dayside low latitude magnetopause crossing. (a) total magnetic field intensity, (b-d) B_X, B_Y and B_Z in aberrated MSM coordinates, (e) the magnetic field zenith (red) and azimuthal (blue) angles, and (f) energy-per-charge spectrogram of FIPS-measured proton flux with a time resolution of 8 s covering the E/q range 0.1 to 13 keV/e. The locations of the magnetosheath (MSH), plasma depletion layers (PDL) and magnetopause (MP) are labeled. The MESSENGER orbit projected onto the aberrated MSM (g) X-Z and (h) X-Y planes relative to Mercury's surface (circle) and the average magnetopause from the model (dashed line).

Figure 2.

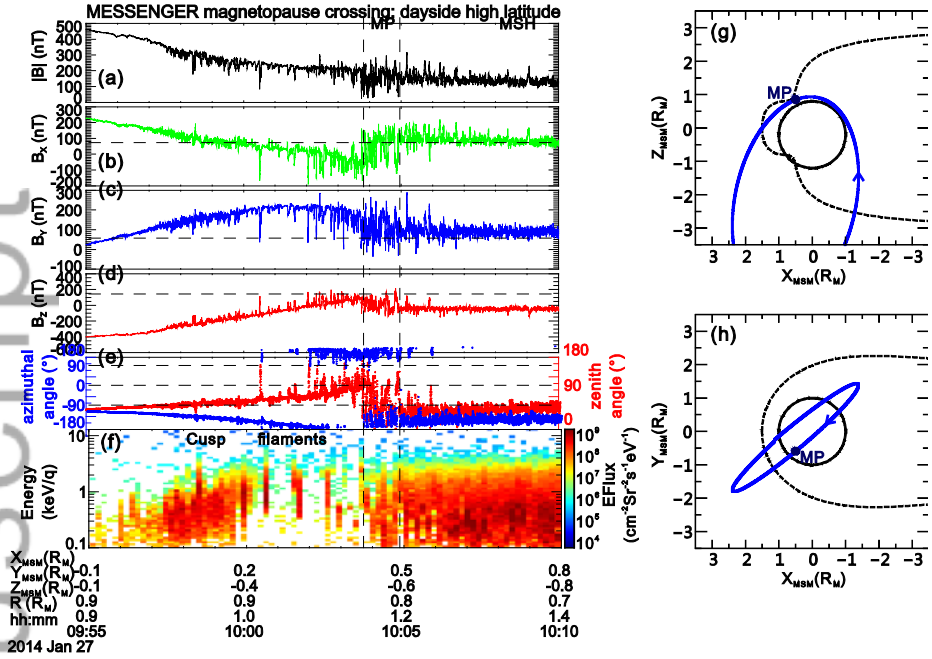

Figure 2. Example of MESSENGER outbound passage from the poleward side of the cusp through the dayside high latitude magnetopause crossings. The locations of the two magnetopause crossings and the cusp region are shown. The layout is the same as in Figure 1.

Figure 3.

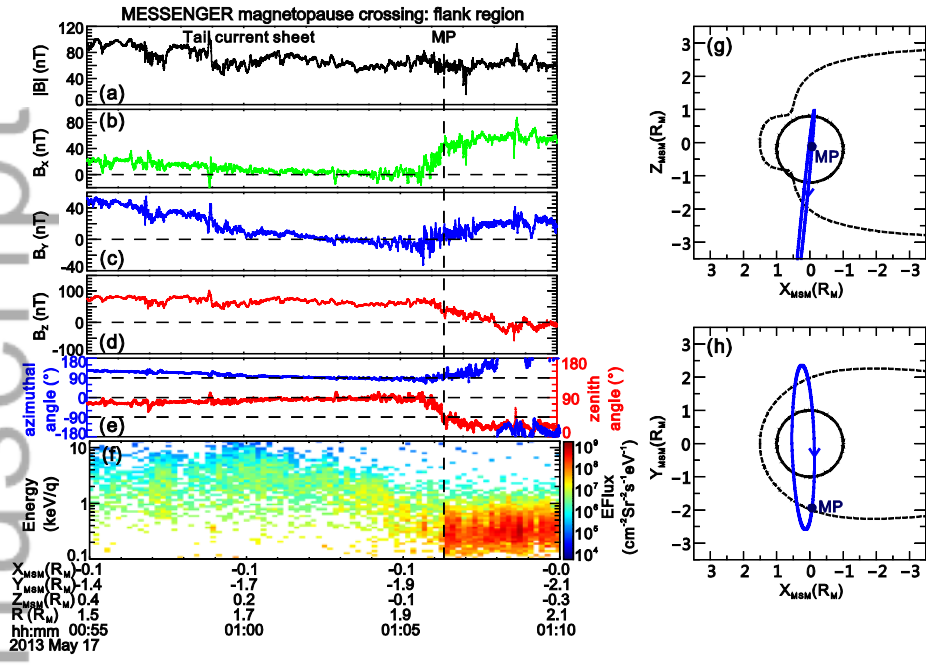

Figure 3. Example of MESSENGER outbound passage from tail current sheet through the magnetopause flank region crossing. The locations of the magnetopause crossing and tail current sheet are shown. The layout is the same as in Figure 1.

Figure 4.

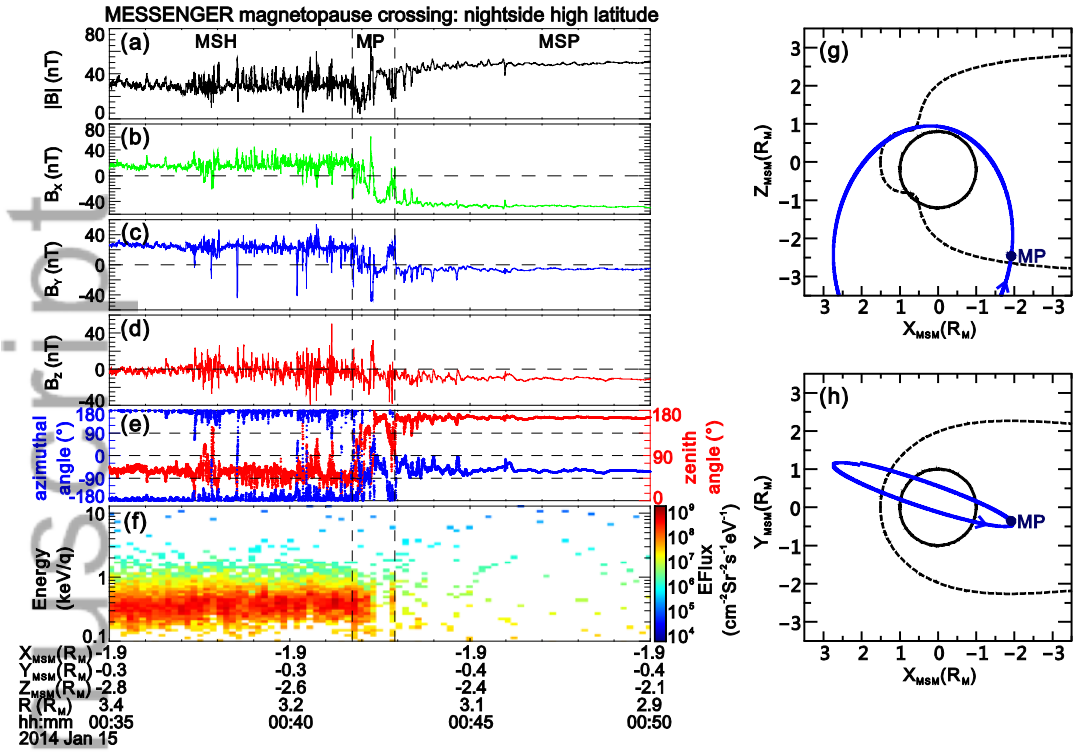

Figure 4. Example of MESSENGER inbound passage from magnetosheath through the nightside high latitude crossings. The locations of the two magnetopause crossings are shown. The layout is the same as in Figure 1.

Figure 5.

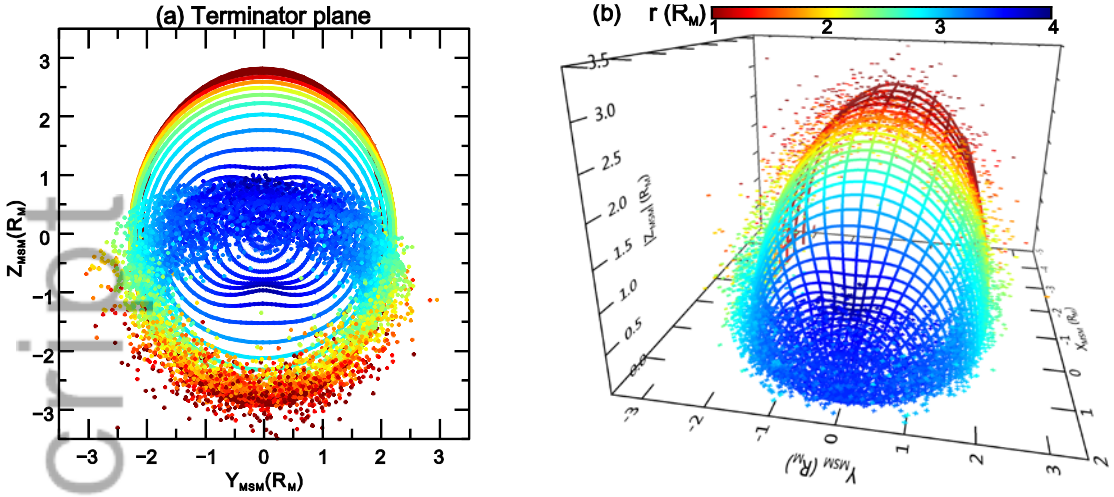

Figure 5. (a) Projection of the MESSENGER magnetopause crossings on the terminator solar-wind-aberrated MSM plane. (b) Magnetopause locations in 3D-view near-Mercury space. The crossing locations in the southern hemisphere are mirrored to the northern hemisphere. The colors show the radial distance from the dipole center. The solid lines are cross sections of the magnetopause at different polar and azimuthal angle from constructed three-dimensional model (see detail in the text). The fitted model parameters are: r_0= 1.51 R_M, α= 0.49, β= −0.10, d_0= 0.64 R_M, θ_0= 1.00 (57.4°), Δ_θ= 0.29 (16.6°) and Δ_φ= 0.48 (27.4°).

Figure 6.

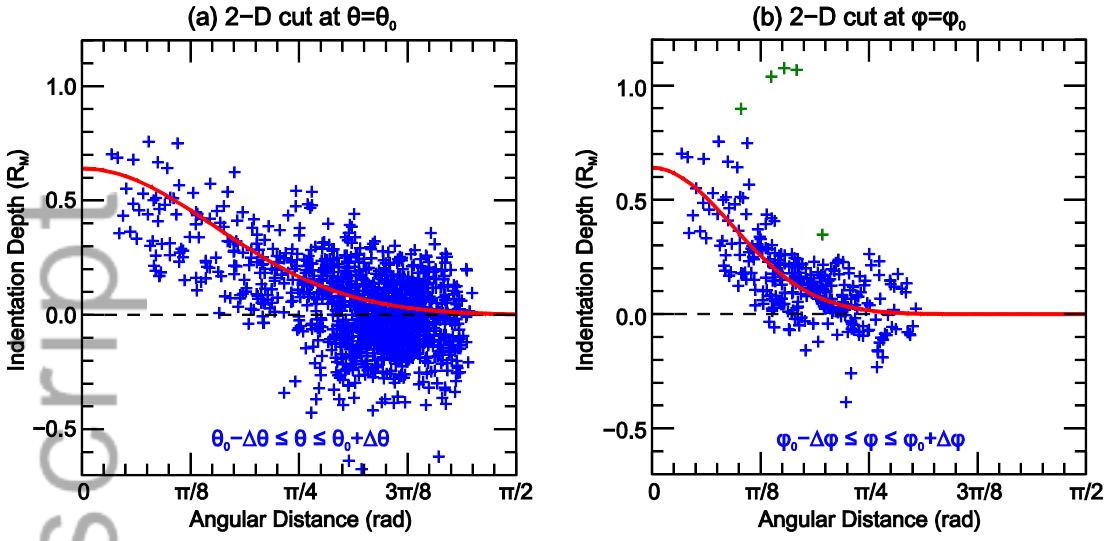

Figure 6. Observations of the Mercury's magnetopause near-cusp indentation depth: (a) near the $\theta = \theta_0$ plane ($|\theta - \theta_0| < \Delta_\theta$), and (b) near the $\varphi = \varphi_0$ plane ($|\varphi - \varphi_0| < \Delta_\varphi$). The near-cusp indentations $r_{ind}(\theta, \varphi)$ are scatter plotted as function of the angular distance from the indentation center, the angle between the radial direction $r(\theta, \varphi)$ and the direction of the indentation center $r(\theta_0, \varphi_0)$ from the model. The solid red lines in (a) and (b) are two-dimensional cut from the model at $\varphi = \varphi_0 = \pi/2$ (noon-midnight plane) and $\theta = \theta_0$ (where θ_0 from the model), respectively.

Figure 7.

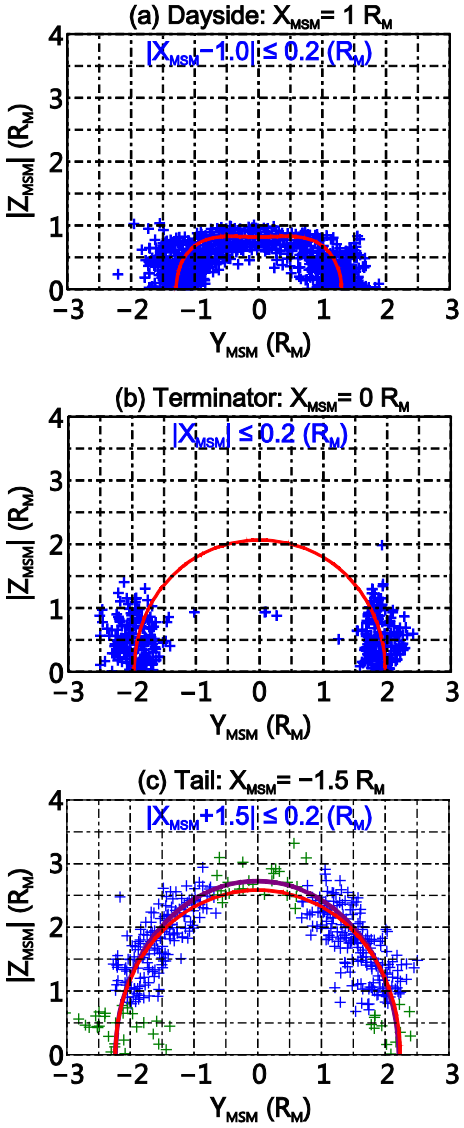

Figure 7. The magnetopause cross section at (a) the dayside X_{MSM}= 1 R_M, (b) the terminator and (c) the nightside X_{MSM}= −1.5 R_M. The crosses are MESSENGER magnetopause crossings and the red lines are Y-Z plane cut from the three-dimensional Mercury's magnetopause model. The middle-latitude of magnetopause crossings at X_{MSM}= −1.5 R_M ($\pi/9 < |\varphi+\pi/2| < 5\pi/12$, blue crosses) are

fitted to an ellipse, which is shown as a purple line in Figure 7c. The fitted ellipse semi-axes are 2.2 R_M and 2.7 R_M in the Y_{MSM} and Z_{MSM} directions, respectively.

Figure 8

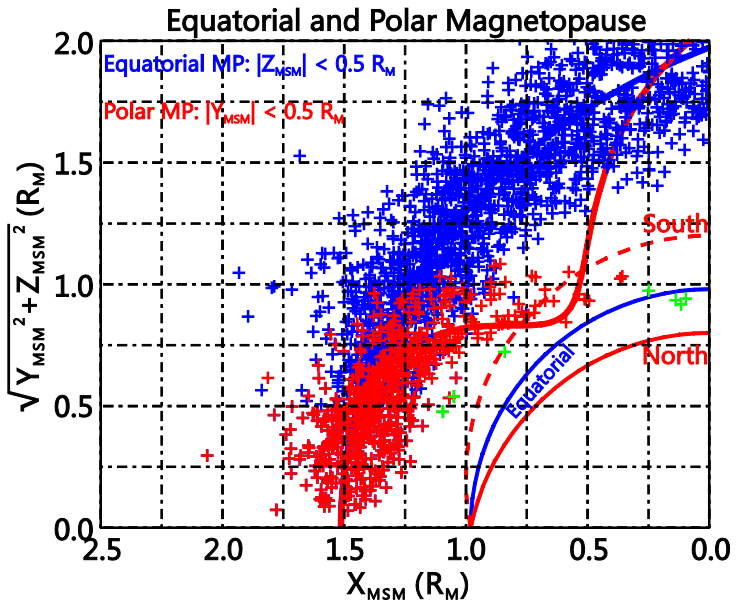

Figure 8. Observations of the Mercury's equatorial magnetopause (blue) and polar magnetopause (red) relative to Mercury's surface. The polar magnetopause crossings during extreme high solar wind pressure events are green colored. The planetary surface north and south of the magnetic equator are labeled. Note the displacement of the planetary center relative to the Z-Y plane because of the northward offset of the magnetic dipole by ~0.2 R_M.

Figure 9.

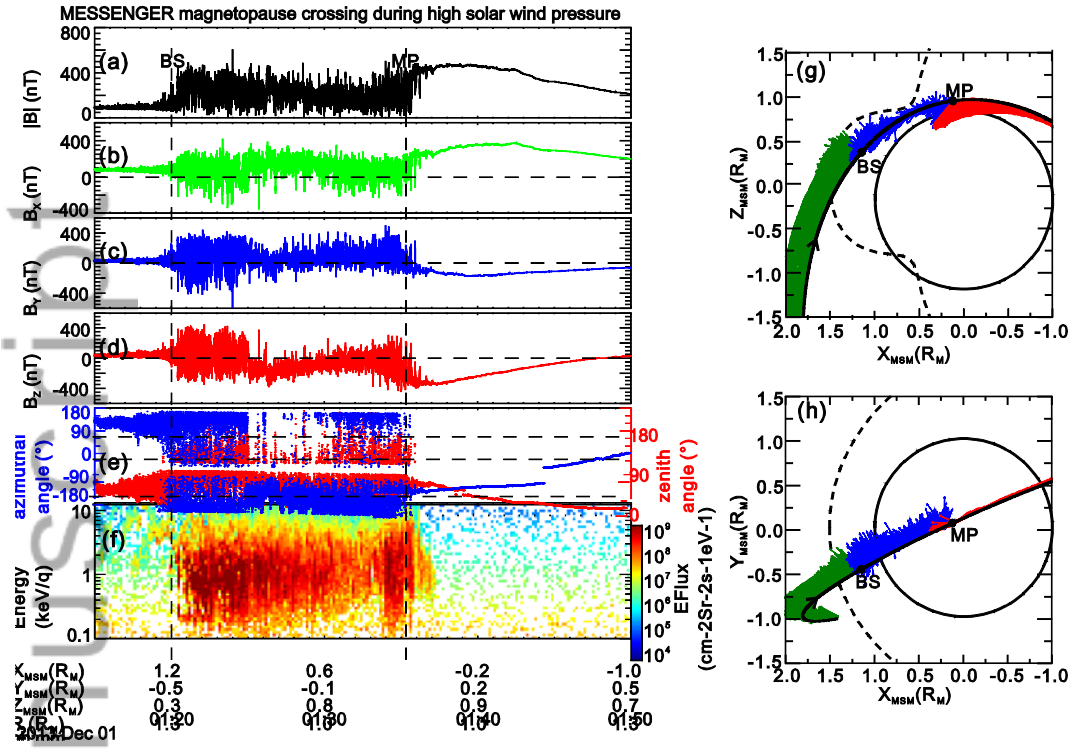

Figure 9. Example of MESSENGER magnetopause crossing during extreme high solar wind pressure event. The layout is the same as in Figure 1. The locations of the bow shock (BS) and magnetopause (MP) crossing are shown. The MESSENGER orbit and the vector plots of the magnetic field in the aberrated MSM (g) X-Z and (h) X-Y planes relative to Mercury's surface (circle) and the average magnetopause from the model (dashed lines).

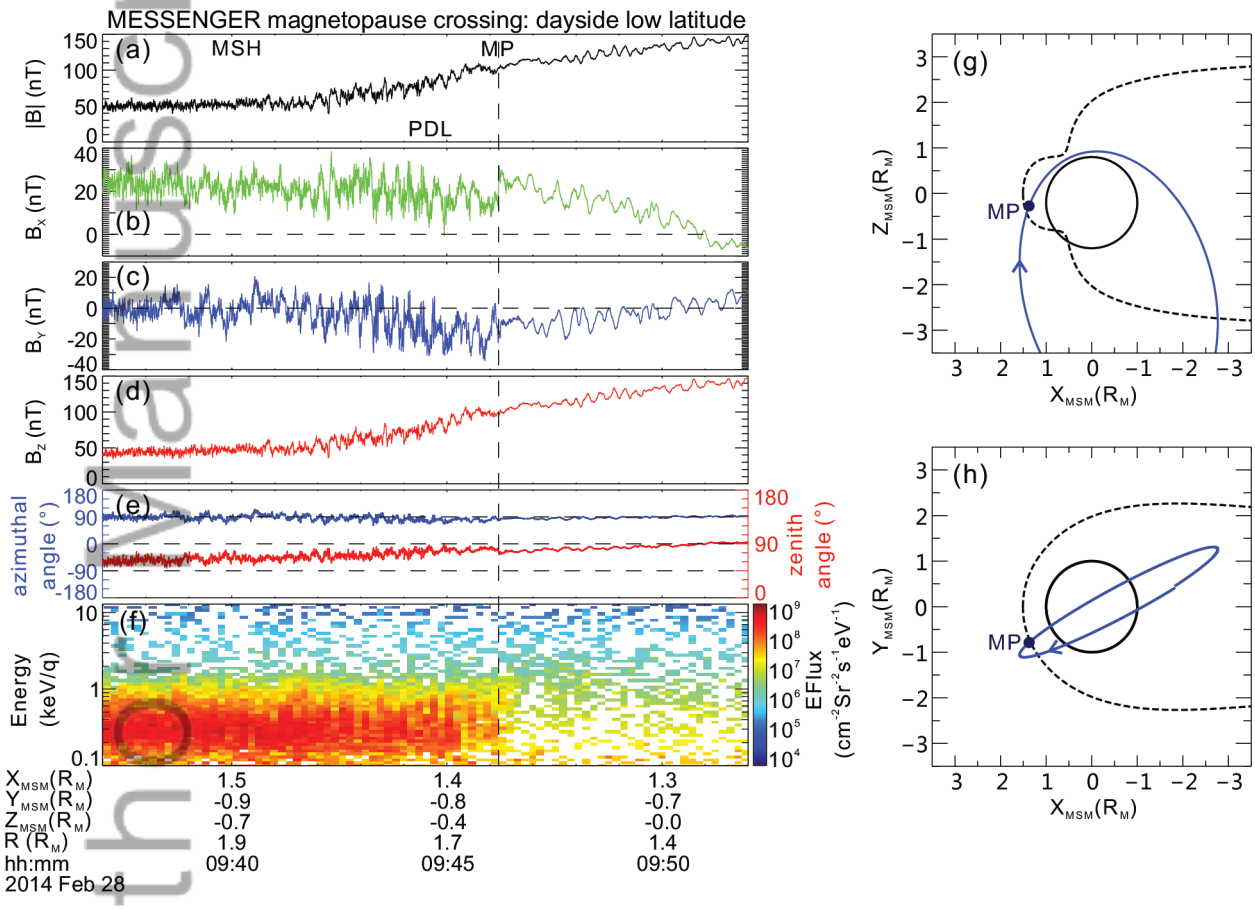

fig_1

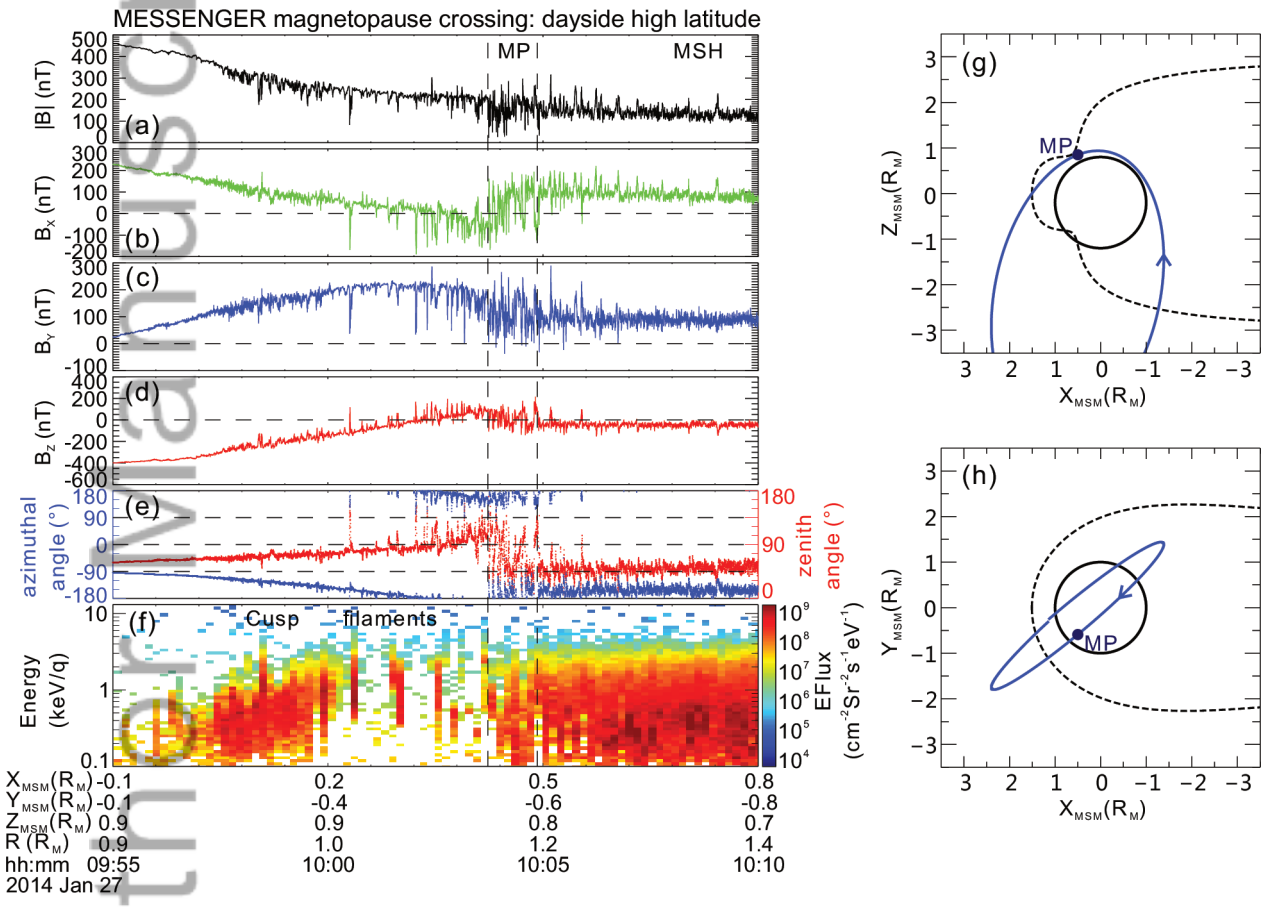

fig_2

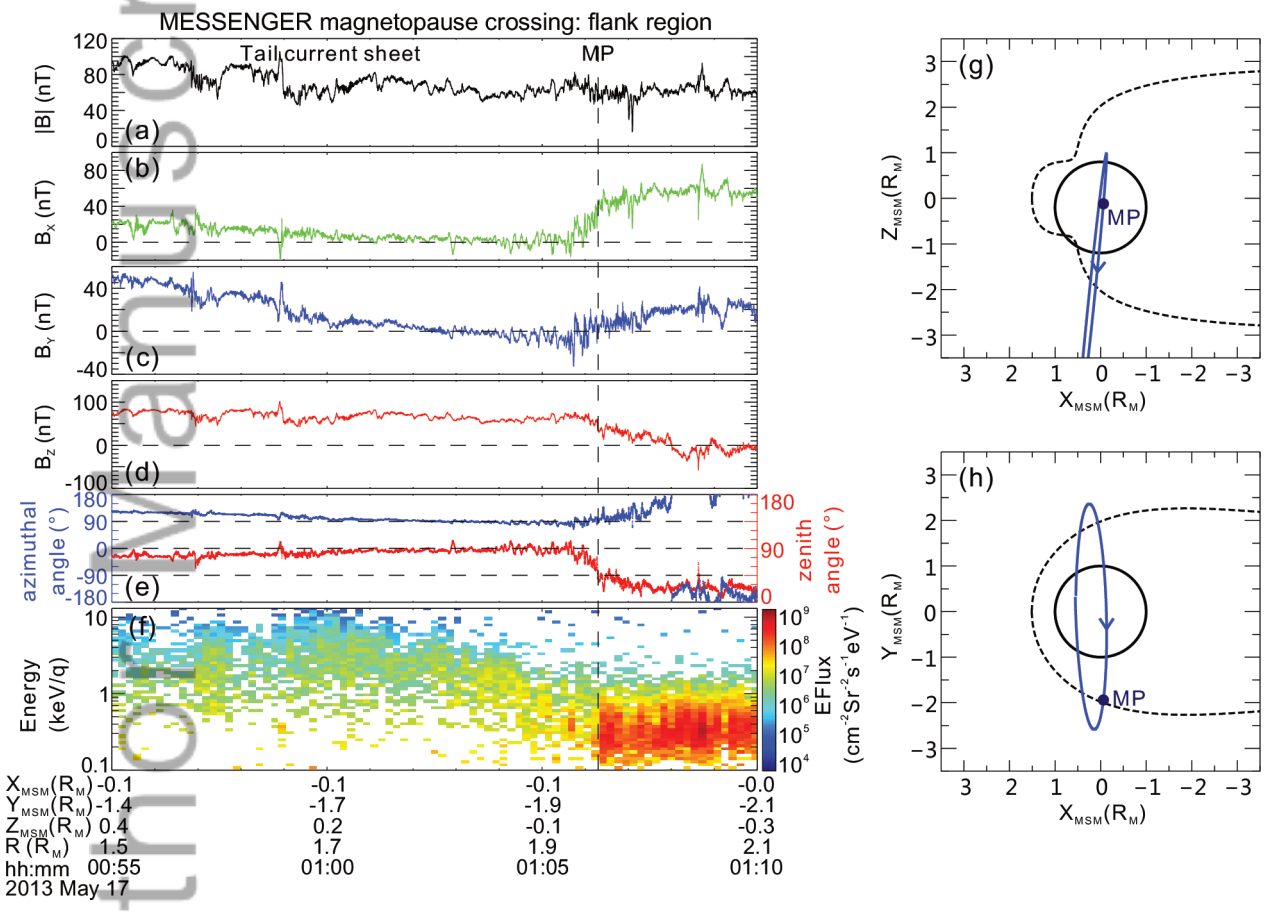

fig_3

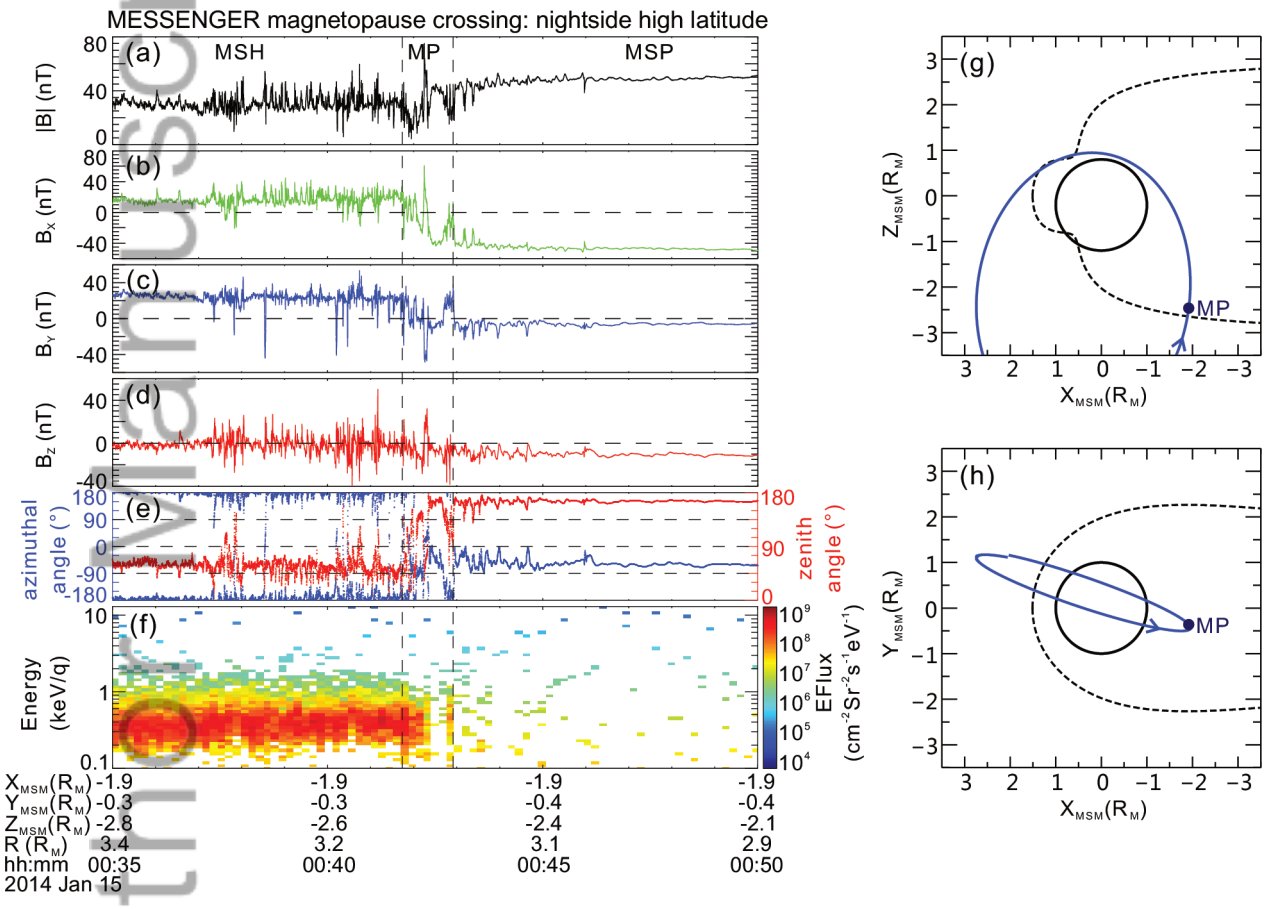

fig_4

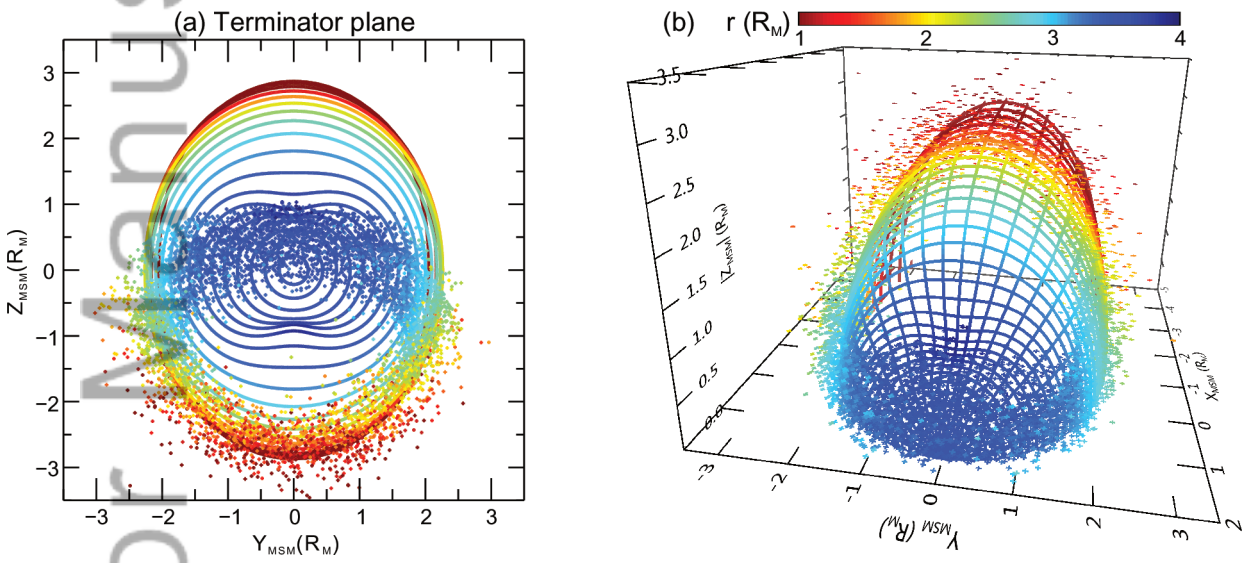

fig_5

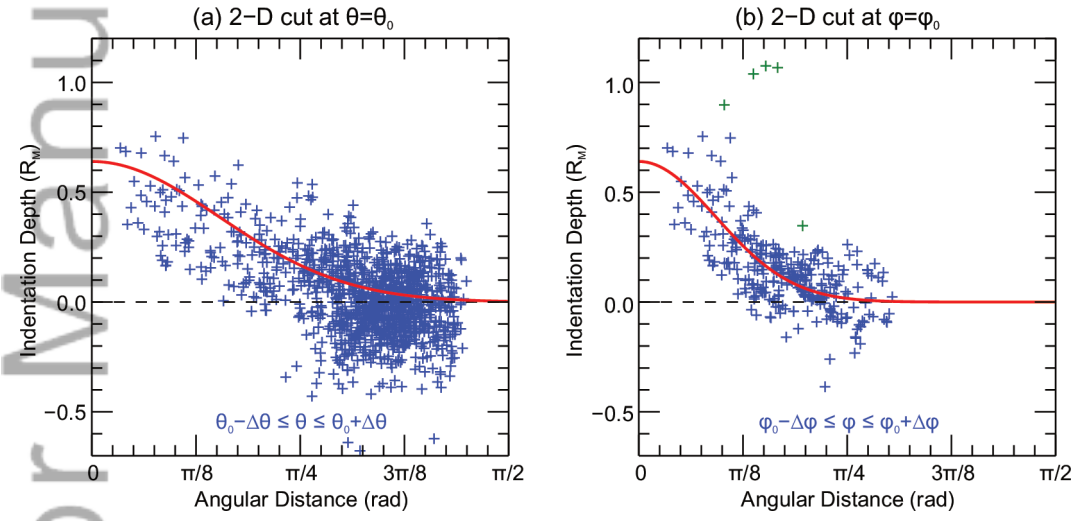

fig_6

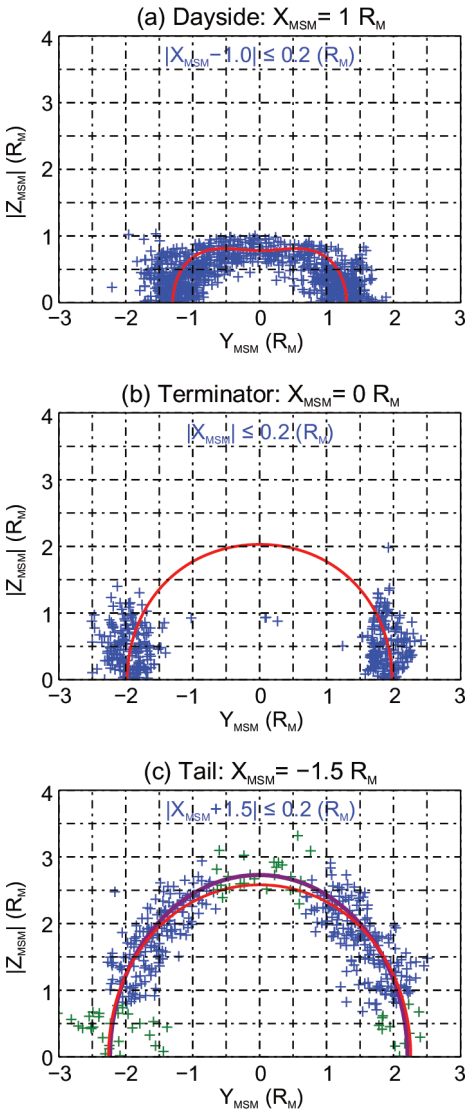

fig_7

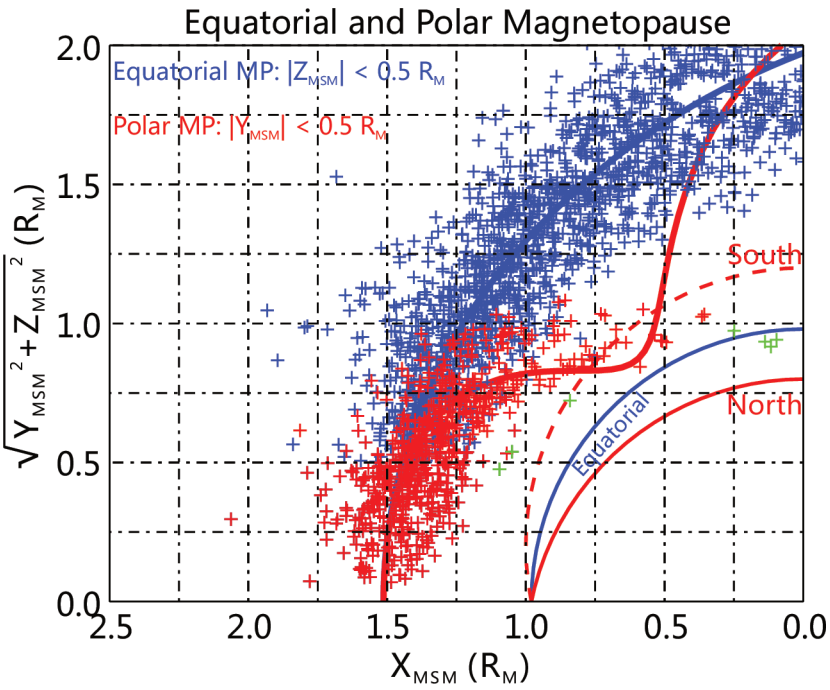

fig_8

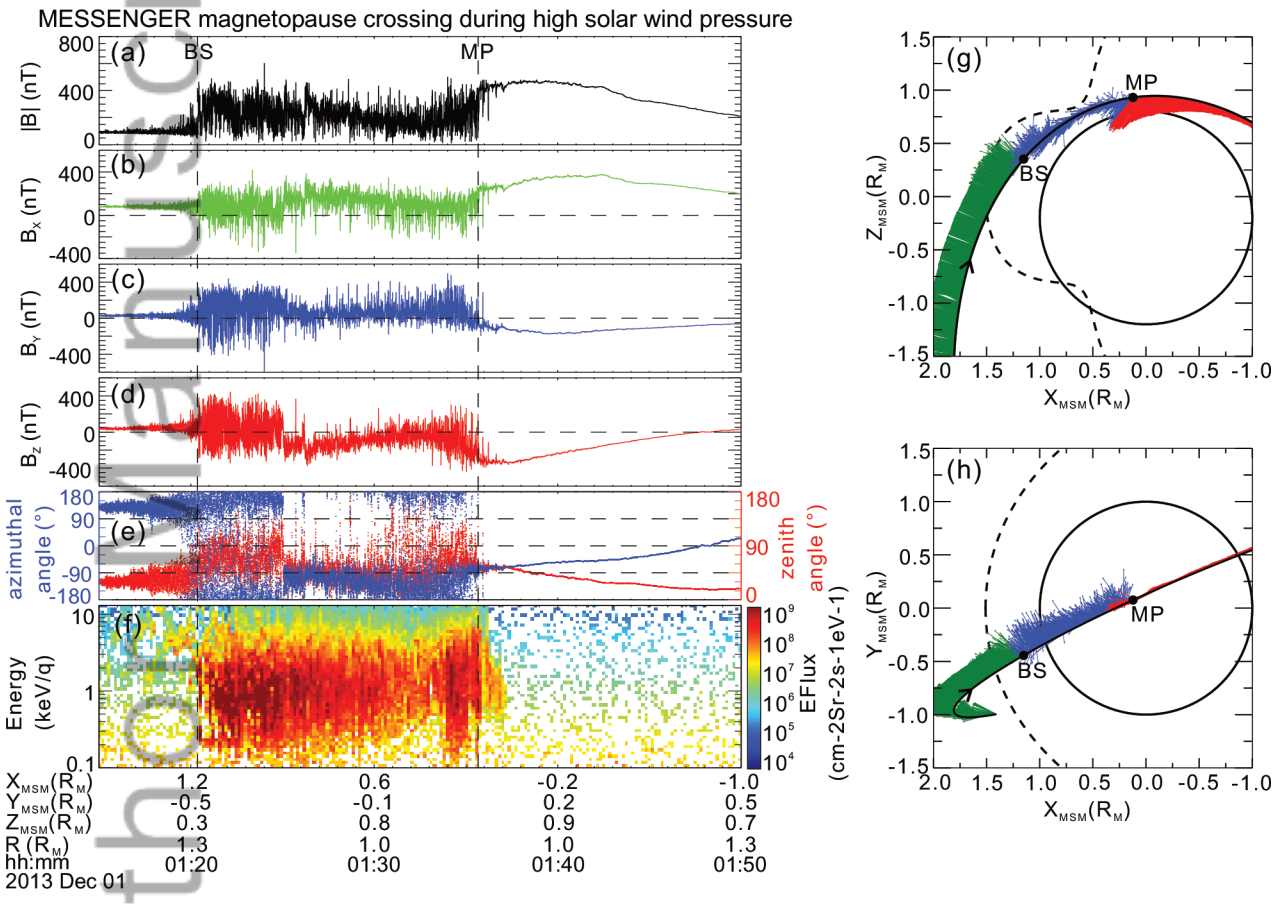

fig_9